Mechanistic Investigations via DFT Support the Cooperative Heterobimetallic C-H and O-H Bond Activation Across Ta=Ir Multiple Bonds

Iker Del rosal, Sébastien Lassalle, Laurent Maron, Chiara Dinoi, Chloé Thieuleux, Clément Camp

ARTICLE

Mechanistic Investigations *via* DFT Support the Cooperative Heterobimetallic C-H and O-H Bond Activation Across Ta=Ir Multiple Bonds

Received 00th January 20xx,
Accepted 00th January 20xx

DOI: 10.1039/x0xx00000x

Iker Del Rosal,[a] Sébastien Lassalle,[b] Chiara Dinoi,[a] Chloé Thieuleux,[b] Laurent Maron[a] and Clément Camp*[b]

A rare heterobimetallic oxidative addition of X-H (X = C, O) bonds is reported. DFT suggests that steric constraints around the bimetallic core play a critical role to synergistically activate C-H bonds across the two metals and thus explains the exceptional H/D exchange catalytic activity of unhindered surface organometallic Ta/Ir species observed experimentally.

Introduction

In recent years, there is a growing interest in transition metal catalysis for the development of heterobimetallic systems able to promote original chemical reactivity which differs from, and ideally surpasses, that of its two monometallic components.[1–9] Although a diverse range of heterobimetallic systems have been described to date, few of them are capable of activating substrates across the two metals simultaneously and, in many cases, the observed reactivity is localized at one metal centre only. This can be explained, in part, by the common use of sterically encumbering polyfunctional chelating ligands to drive the assembly of the two metals, which restrains the accessibility of both metal cores, therefore limiting their interest for catalysis.

Still, rare examples of heterobimetallic oxidative additions (HBOA) of H-H,[10–15] C-X (X = halide,[16,17] H,[18–22] OH,[23–26] NHR,[23–25]), Si-H[24] or B-H[27] bonds across metal-metal' bonds have emerged in the literature (see Figure 1). These pioneer studies highlight the potential of polarized heterobimetallic metal-metal bonds to promote the cooperative cleavage of strong sigma bonds. Yet, there is still an immense lack of knowledge on the factors governing these HBOA processes which impedes the thoughtful design of novel heterobimetallic complexes for targeted applications in catalysis.

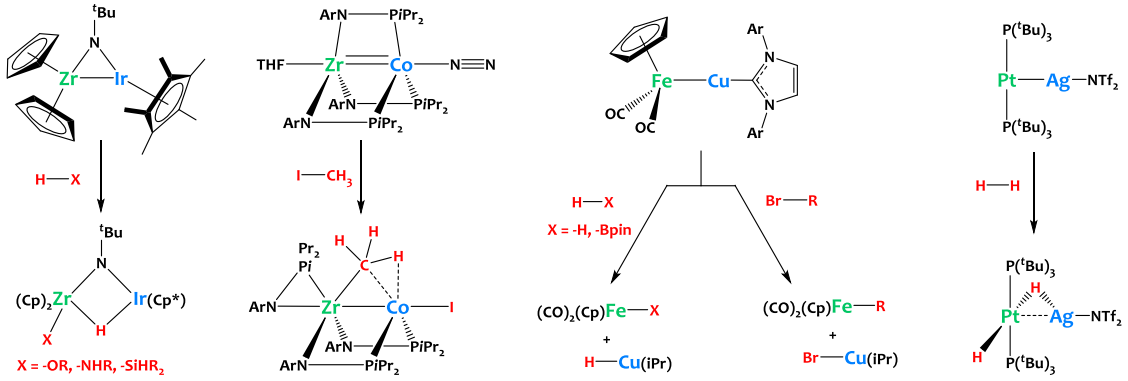

Figure 1. Representative heterobimetallic oxidative additions at metal-metal bonds.

In the quest for potential candidates to promote unconventional C-H bond activations, we identified heterobimetallic complexes formed by alkane elimination as attractive prospects. This reaction involving a nucleophilic metal alkyl derivative and a Brønsted acidic metal hydride (Scheme 1) is a useful synthetic tool – yet rarely used – to generate original species featuring metal-metal bonds.[28–30] We hypothesized that such systems might be, by virtue of the

[a] Université de Toulouse et CNRS, INSA, UPS, UMR 5215, LPCNO, 135 Avenue de Rangueil, F-31077 Toulouse, France.
[b] Laboratory of Chemistry, Catalysis, Polymers and Processes, C2P2 UMR 5265, Université de Lyon, Institut de Chimie de Lyon, CNRS, Université Lyon 1, CPE Lyon, 43 Bd du 11 Novembre 1918, F-69616 Villeurbanne, France. E-mail: clement.camp@univ-lyon1.fr

Electronic Supplementary Information (ESI) available: [experimental and computational details]. See DOI: 10.1039/x0xx00000x

principle of microscopic reversibility (Scheme 1), particularly well poised to promote the reverse reaction, i.e. the heterolytic cleavage of unactivated C-H bonds through unusual cooperative metal-metal pathways.

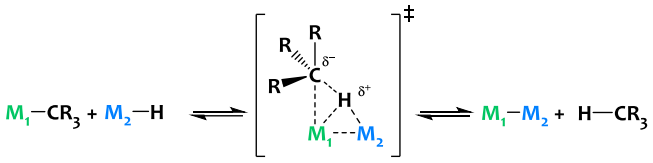

Scheme1. Alkane elimination reaction.

Based on this mechanistic blueprint we investigated and reported in a preliminary study the alkane elimination reaction between the tantalum *tris*alkyl(alkylidene) $Ta(CH^tBu)(CH_2{}^tBu)_3$ and the iridium polyhydride $Ir(Cp^*)H_4$ as a method to isolate rare examples of heterobimetallic tantalum-iridium complexes in solution (complex **1**) and immobilized at the surface of silica materials (species **2** and **3**), shown on Figure 2.[31,32]

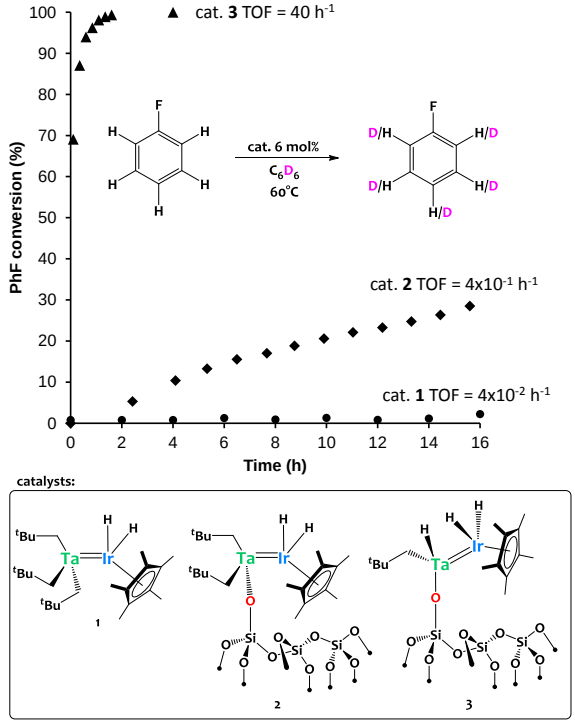

Figure 2. Catalytic H/D exchange reaction, productivity and structure of the Ta/Ir catalysts **1-3** (bottom), reproduced according to ref.[31]

To our delight, these systems featuring multiple metal-metal bonds catalysed the H/D isotopic exchange of arene C-H bonds. Evidence for metal-metal synergistic effects was gained by comparing the catalytic activity of the tantalum/iridium heterobimetallic species **1-3** with that of monometallic analogues. $Ta(CH^tBu)(CH_2{}^tBu)_3$, Cp^*IrH_4 and $[(\equiv SiO)Ta(CH^tBu)(CH_2{}^tBu)_2]$ gave no productive catalysis while $[(\equiv SiO)_2TaH_n]$ exhibited significantly lower activity in comparison with **2-3**.[31] Moreover, the use of the silica support has a drastic impact on the catalytic performances: the catalytic activity of the immobilized species **3** rivals those of the best catalytic systems known to date,[33–35] and is two orders of magnitude higher than that of the homogeneous analogue, **1**.[31] It is important to note that this difference in activity is not due to deactivation phenomena since **1** is stable in the course of catalysis and high conversions (>74%) can be reached with catalyst **1** at higher temperature (110°C).

Experimental

General considerations.

The synthesis was performed under an argon atmosphere. Glassware was stored in an oven at ~100 °C for at least 12 h prior to use. The solvents were purified by passage through a column of activated alumina, dried over Na/benzophenone, vacuum-transferred to a storage flask and freeze-pump-thaw degassed prior to use. Complex **1** was prepared according to the reported literature procedure.[31] All other reagents were acquired from commercial sources and used as received.

Preparation of $[(ArO)_4Ta(H)_3IrCp^*]$ (Ar = 2,6-$(CH_3)C_6H_3O$), 4.

In an argon-filled glovebox, a colourless solution of xylenol (67.4 mg, 0.552 mmol, 4 eq.) in pentane (4 mL) was slowly added dropwise to an orange solution of complex **1** (100.2 mg, 0.138 mmol, 1 eq.) in pentane (4 mL) at room temperature. The solution gradually turned from orange to yellow and the formation of a beige precipitate was observed. After 19h of stirring at room temperature the beige precipitate was recovered by filtration and dried under vacuum leading to a beige solid. The beige solid was solubilized in a pentane (12 mL) and toluene (5 mL) mixture and stored at -38°C for 2 days leading to colourless crystals. The colourless liquid supernatant was removed and the crystals were dried for 2h under vacuum leading to [**4**•toluene] as a white crystalline solid (113 mg, 0.113 mmol, 82 % yield). Single crystals suitable for X-ray diffraction were grown similarly. ^1H NMR (25°C, 500MHz, C_6D_6) δ 6.88 (d, 8H, CH_{Ar}, *J*=6 Hz), 6.68 (t, 4H, CH_{Ar}, *J*=6 Hz), 2.40 (s, 24H, $CH_3$from xylenolate), 1.82 (s, 15H, $CH_3$from Cp*), -10.75 (s, 3H, Ir-H). $^{13}C\{^1H\}$ NMR (25°C, 101 MHz, C_6D_6) δ 161.28 (*i*-C_{Ar}), 128.33 (*m*-C_{Ar}), 127.35 (*o*-C_{Ar}), 121.09 (*p*-C_{Ar}), 97.11 (Cp*), 18.62 (CH_3xylenolate), 10.41 (CH_3Cp*). DRIFT (293K, cm^{-1}) 3063 (m, *ν*C-H), 3012 (m, *ν*C-H), 2947 (s, *ν*C-H), 2911 (s, *ν*C-H), 2848 (m, *ν*C-H), 2103 (s, *ν*Ir-H), 1587 (s), 1465 (s), 1421 (s), 1383 (m), 1296 (s), 1267 (s), 1215 (s), 1089 (w), 1027 (m), 880 (s). Elemental analysis calcd. (%) for $C_{49}H_{62}O_4TaIr$: C 54.08, H 5.74; Found C 54.19, H 5.67.

DFT calculations

All DFT calculations were carried out with the Gaussian 09 suite of programs. Geometries were fully optimized in gas phase without symmetry constraints, employing the B3PW91 functional.[36,37] The nature of the extrema was verified by analytical frequency calculations. The calculation of electronic energies and enthalpies of the extrema of the potential energy surface (minima and transition states) were performed at the same level of theory as the geometry optimizations. IRC calculations were performed to confirm the connections of the

optimized transition states. Iridium and Tantalum atoms were treated with a small-core effective core potential (60 MWB), associated with its adapted basis set[38] augmented with a polarization function (ζ_f = 0.938 and 0.790 respectively for Ir and Ta). Si atoms were treated with a Stuttgart effective core potential[39] augmented with a polarization function (ζ_d = 0.284).[40] For the other elements (H, C and O), Pople's double-ζ basis set 6-31G(d,p) was used.[41–44] The electronic charges (at the DFT level) were computed using the natural population analysis (NPA) technique.[45] Some reactant intermediates and transition states were additionally optimized including solvent effect and dispersion corrections (Table S2). More precisely, dispersion corrections were treated with the D3 version of Grimme's dispersion with Becke-Johnson damping.[46] Solvent effect was evaluated by using SMD solvation model.[47] Benzene was used as solvent.

Results and Discussion

In order to better understand the reaction mechanism operating in these heterobimetallic systems as well as the role of the solid support, DFT calculations (B3PW91) were carried out on the H/D scrambling of benzene catalysed by complexes **1**, **2** and **3**. The first step of the reaction is the C-H activation of benzene and is found to be an HBOA over the Ta=Ir bond (Figure 3) with the phenyl interacting with the tantalum centre and the hydrogen bridging the Ta-Ir bond. It should be mentioned that several other mechanistic possibilities were considered and found to be higher in energy (see Figures S5, S6 and S7).

As can be seen, the oxidative addition barrier is decreasing in the same order as the experimental activity increases (Figure 4), namely the homogeneous complex **1** being the least active and complex **3** being the most active. The charge distribution is of great importance in order to understand the stability of the oxidative addition barrier. However, in the present case, as illustrated in Figure 3, the charge alteration is almost the same with the three complexes. Thus, the origin of the difference on the height of the HBOA barriers is unlikely to be electronic, but is mostly explained by sterics at the transition state.

For complex **1**, due to the steric hindrance around the tantalum centre imposed by the bulky neopentyl (Np) substituents, the approach of the substrate is difficult and the Ta-Ph distance is long (2.53 Å), inducing a low stabilization of the TS. Therefore, the C-H bond has to be strongly activated (1.49 Å) in order to get a stabilizing Ir-H interaction (1.82 Å). The oxidative C-H addition is thus involving more Ir than Ta because of the steric hindrance but this implies to have a strongly activated C-H bond which requires energy. On the other hand for complex **2**, the replacement of one Np group by the silica surface allows to reduce the steric hindrance around Ta so that the Ta-Ph distance is slightly decreased (2.49 Å). Consequently, the CH bond is less activated (1.40 Å) because the implication of Ir is reduced (Ir-H distance of 1.89 Å). Reducing further the steric hindrance by replacing another Np substituent by a simple hydride allows to improve the participation of Ta by decreasing the Ta-Ph distance to 2.41 Å but also by allowing an H more uniformly bridging the Ta-Ir bond (equal Ta-H and Ir-H bond distances of 1.97 Å – note that Ta and Ir have different metallic radii of 1.343 Å and 1.260 Å respectively).[48]

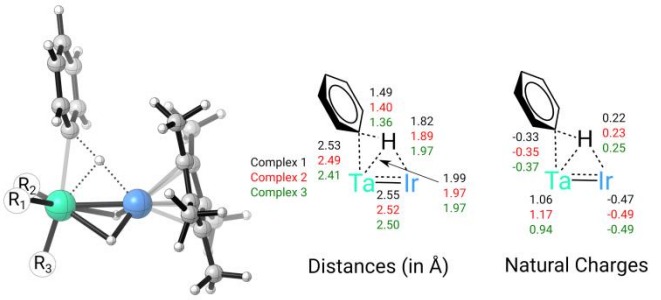

Figure 3. 3D representation of the geometry of the transition state of the bimetallic C-H activation together with the key distances and the Natural Charges. Complex **1**: R_1=R_2=R_3=$CH_2{}^tBu$; complex **2**: R_1=R_2=$CH_2{}^tBu$ and R_3=O-Si≡$_{surface}$; complex **3**: R_1=$CH_2{}^tBu$, R_2=H and R_3=O-Si≡$_{surface}$.

In brief, the heterobimetallic C-H bond oxidative addition is more favourable when the Ta centre is accessible, while the iridium centre is crucial to ensure a nucleophilic assistance, and this is governed by steric hindrance. Quite importantly, this investigation highlights the benefits of the surface organometallic chemistry approach,[49] which allows access to unique unsaturated species not attainable in solution thanks to the solid-support. The resulting low steric hindrance in these supported heterobimetallic edifices is found to be key for reactivity by favouring the HBOA process. This is further highlighted by analysing the HOMO of all systems at the transition state (see Figures 5 and S8). Indeed, the HOMO is clearly describing the formation of the Ta-C bond and of the Ir-H one in line with donation from a filled *d* orbital on Ir to the CH σ* orbital. The donation from the CH σ orbital to an empty *d* orbital on Ta can also be observed on the HOMO-5 orbital of the three complexes. The HOMO and the HOMO-5 of the three systems are lying in the same energy range (-0.19 a.u. and -0.25 a.u., respectively) so that the difference can be safely attributed to steric effects.

Note that this mechanism is reminiscent of the activation of C-H bonds *via* 1,2-addition/elimination to multiple bonds in early transition metal imides and alkylidenes/alkylidynes.[53–63]

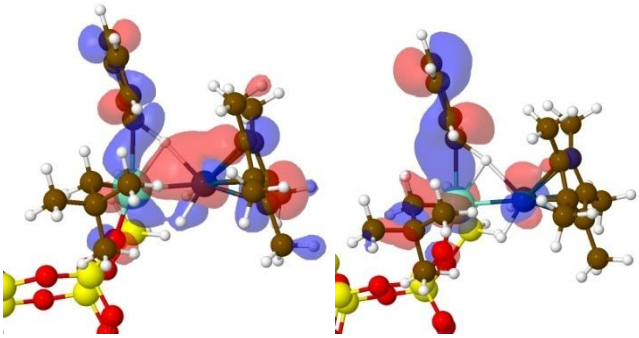

Figure 5. HOMO (left) and **HOMO-5** (right) orbital of the C-H activation transition state from species **3.**

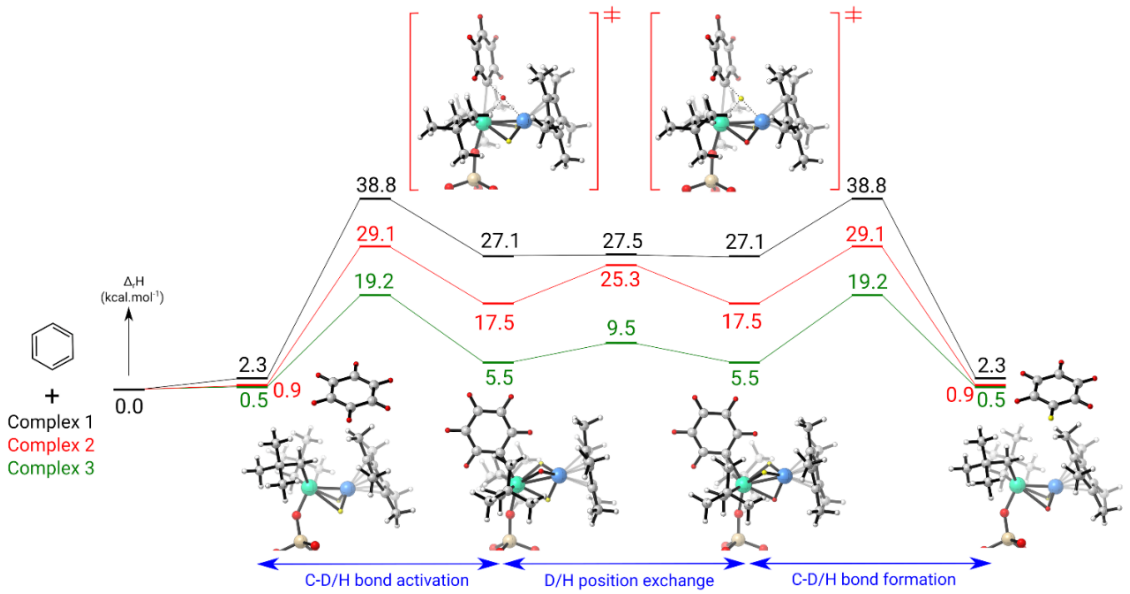

Figure 4. Computed enthalpy profile at room temperature for the H-D exchange of benzene catalyzed by complexes **1**, **2** and **3**.

Following the intrinsic reaction coordinate from the oxidative addition TS, it yields the formation of the C-H oxidative activation product where the three hydrides were found to bridge the Ta-Ir bond. The linear structures with three bridging hydrides are slightly favoured by 2.0 to 3.6 kcal/mol with respect to the tilted structures with two bridging hydrides and one terminal iridium hydride (Figures 6a and S10). As we can see on Figure 4, the formation of the C-H oxidative activation products is found to be endothermic (by 27.1, 17.5 and 5.5 kcal/mol respectively for complexes **1**, **2** and **3**) so that the oxidative addition is reversible. Quite interestingly, the stability of this product follows the same trend as the oxidative addition barrier, the lower the barrier the more stable is the oxidative addition product. Even though the oxidative addition product is fairly unstable, a rotation of the bridging hydrogens is computed to occur easily with barriers that are lower than the reverse of the oxidative addition (0.4 *vs* 11.7 kcal/mol for complex **1**, 7.8 *vs* 11.6 kcal/mol for complex **2** and 4.0 *vs* 13.7 kcal/mol for complex **3**). Thus, in this mechanism, the first key parameter is the height of the HBOA barriers. A second key parameter is the competition between the reverse of the oxidative addition and a rotation of the bridging hydrogens. Indeed, the H/D exchange reaction is only possible if this rotation occurs. This finding is crucial to explain the H/D scrambling observed experimentally. For complex **2** there is slight preference for the hydride rotation (7.8 kcal.mol) *vs* reductive elimination of benzene (11.6 kcal.mol), but still a kinetic competition between the two reactions. For complex **3**, the reductive elimination barrier is 13.7 kcal/mol whereas the hydrides rotation one is only 3.0 kcal/mol so that the H/D exchange is favoured, further increasing the TOF.

It should be noticed that the inclusion of solvent and dispersion effects do not change the conclusion (see table S2 in ESI).[50–52] The inclusion of these effects leads to a decrease of the different activation barriers from 6 to 15 kcal/mol and to the stabilization of the C-H oxidative activation products from 5 to 12 kcal/mol. In this case, according to the oxidative addition barrier, the homogeneous complex **1** remains the least active and complexes **2** and **3** should have a similar activity. However, a lower activity is expected for complex **2** with respect to complex **3**, as observed experimentally, due to the small barrier for the reverse reaction of the oxidative addition (only 4.3 kcal/mol for complex **2** *vs* 12.4 kcal/mol for complex **3**), which reduces the efficiency of the hydrides rotation for **2** and thus the overall H/D exchange reaction.

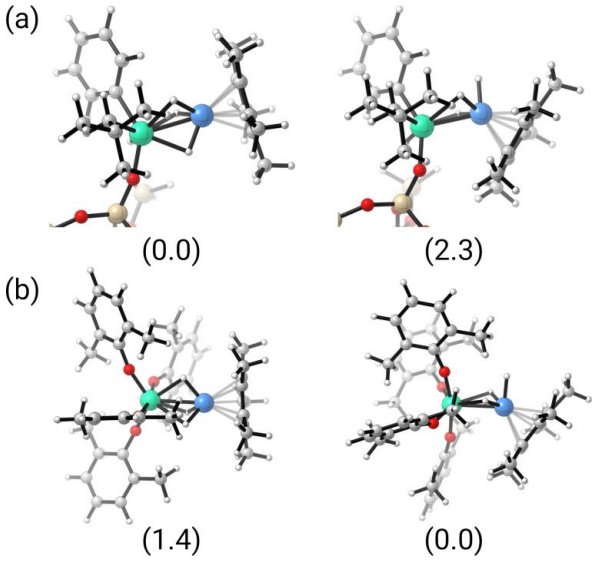

Figure 6. Optimized structures for the X-H addition products catalysed by **3** (a, X = C) as well as complex **4** (b, X = O) and their relative energies (kcal/mol).

Even if the C-H oxidative addition product cannot be trapped – since the process is thermodynamically unfavourable and reversible – addition of a phenolic O-H bond across the Ta=Ir double bond was observed experimentally. Treatment of **1** with 4 equivalents of 2,6-dimethylphenol yields the tris-hydride complex $[(ArO)_4Ta(H)_3IrCp^*]$ (Ar = 2,6-$(CH_3)C_6H_3O$), **4**, in excellent yields (Scheme 2).

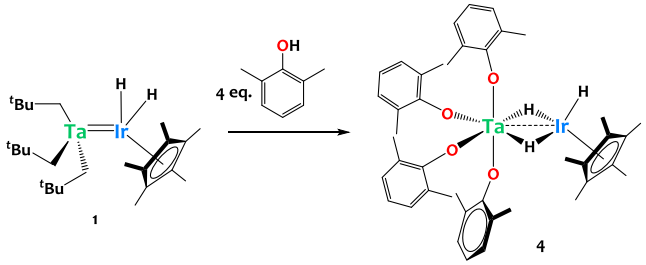

Scheme 2. Heterobimetallic oxidative addition of a O-H bond across the Ta=Ir double bond from **1**.

The ^{1}H NMR spectrum for **4** (Figure S1) displays a characteristic signal at -10.8 ppm integrating for 3H, corresponding to the three hydrides in **4**, which are equivalent on the NMR time scale at room temperature. Rapid exchange between the three hydrides is not unexpected on the basis of literature precedents for metal-polyhydride systems.[32,64,65] The IR spectrum of **4** (Figure S3) shows a distinct absorption at 2103 cm^{-1}, which is assigned to a Ir-H stretching vibration.[31,32,66–68] The identity of **4** was supported by single-crystal X-ray diffraction. The solid-state structure of **4**, shown on Figure 7, confirms the coordination of four phenoxides to the Ta centre. The intermetallic Ta-Ir distance in **2** is quite short (2.5926(2) Å) but is elongated by 0.23 Å in comparison with that found in **1** (2.3559(6) Å), which features a Ta=Ir double bond.[31] The close Ta-Ir proximity in **4** is most likely the result of the presence of bridging hydride ligands, although a metal-metal interaction cannot be excluded since the Ta-Ir distance is in the range of the sum of the respective metallic radii (2.603 Å; FSR = 0.99)[31] and falls in the range of the few reported Ta-Ir bonds (2.43-2.85 Å).[21,25,31,69,70] The acute tilting of the Cp* ligand with respect to the Ta-Ir axis (Ta-Ir-Cp* centroid = 141.3(1)) seems to indicate the presence of a terminal iridium hydride as well. Even if the hydrides could not be precisely located in the Fourier difference map of the crystal structure of **4**, hint of their presence is thus given by the analysis of the metrical parameters. Furthermore this coordination environment and geometry in **4** is confirmed computationally (see below).

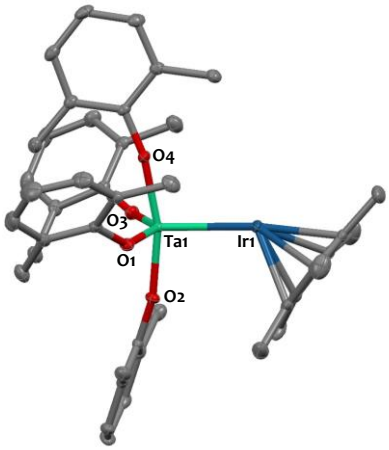

Figure 7. Solid-state molecular structure of **4** (30% probability ellipsoids). Interstitial toluene solvent molecule and hydrogen atoms have been omitted for clarity. Selected bond distances (Å) and angles (°): Ta1-Ir1 2.5926(2), Ta1-O1 1.925(2), Ta1-O2 1.907(2), Ta1-O3 1.916(2), Ta1-O4 1.926(2), Ta1-Ir1-$Cp^*_{centroid}$ 141.3(1) .

Complex **4** is the result of the classical protonolysis of the three neopentyls from **1**,[31,32,71,72] leading to the formation of phenoxides, as well as the HBOA of the fourth equivalent of phenol across the Ta=Ir bond. Note that when **1** is treated with less than 4 eq. ArOH *per* Ta site, intractable mixture of species are formed, as a result of the competition between the multiple protonolysis reactions which leads to a distribution of mono-, di- and tri-substituted species along with unreacted **1**. The mono-substituted complex $[\{Ta(OAr)(CH_2{}^tBu)_2\}\{IrH_2(Cp^*)\}]$ (OAr = 2,6-$(Ph)_2$-C_6H_3O), can only be accessed when 1 eq. of the more bulky 2,6-diphenylphenol is used in place of 2,6-dimethylphenol to avoid polysubstitution, as reported before.[31]

The formation of complex **4** by the HBOA of the fourth equivalent of phenol across the Ta=Ir bond has also been theoretically studied. As we can see on Figure 8, this reaction is kinetically accessible with a low activation barrier (between 6.4 and 12.6 kcal/mol according to the coordination site of the ArOH substrate). At the transition state, the transferred hydrogen is bridging the Ta-Ir bond (Ta-H distance of 2.18 Å and Ir-H of 1.93 Å) so that the oxidative addition occurs in a concerted manner. The formation of **4** is found to be exothermic by 18.7 kcal/mol. Overall these computations suggest that the O-H addition is mechanistically related to the C-H addition described above. The structure of complex **4** was analysed in details in order to check the stability of the structure when the number of bridging hydride is changed from two to three. Computationally, the structures with either two or three bridging hydrides were found to be stable with a very small energy preference (1.4 kcal/mol which lies within the precision of the method) for the bent form with two bridging hydrides (Figure 6b and 8) as found experimentally in the solid-state. Thus one can conclude that there is an equilibrium in solution between the two structures.

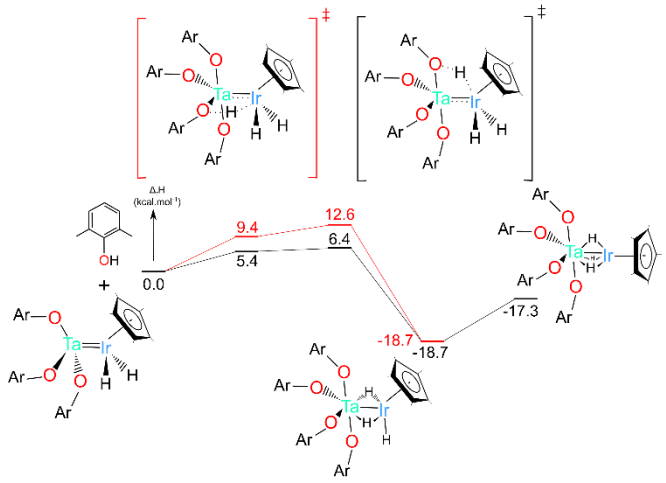

Figure 8. Heterobimetallic oxidative addition of a O-H bond across the Ta=Ir double bond (OAr = 2,6-$(Me)_2$-C_6H_3O).

Conclusions

In summary, a rare concerted heterobimetallic oxidative addition process of X-H (X = C, O) bonds across the early/late Ta=Ir double bond is supported by experimental and computational data. The analysis of the transition state structure shows the critical role of the bimetallic core in these systems to realize the unusual synergistic activation of C-H and O-H bonds. This study also confirms the drastic impact of steric effects on the reactivity of heterobimetallic systems, and the reactivity trend observed experimentally is reproduced computationally. This highlight the benefits of surface organometallic chemistry to access unique bimetallic cores with low steric profile - which could not be obtained in solution - through the use a solid support. We believe that the mechanistic understanding of these bimetallic bond activations will stimulate progress in the field and will help designing a second-generation of systems. Future efforts will be devoted in our group to extend this chemistry to other couples of metals using a similar alkane elimination synthetic methodology to study the impact of the nature of the two metals in these heterobimetallic C-H oxidative addition processes.

Conflicts of interest

There are no conflicts to declare.

Acknowledgements

We thank Tanya K. Todorova for helpful discussions, Pauline Schiltz for preliminary investigations and Erwann Jeanneau for the XRD analysis. LM is a senior member of the Institut Universitaire de France. This work was supported by the CNRS-MOMENTUM 2017 program. The authors acknowledge the HPCs CALcul en Midi-Pyrénées (CALMIP-EOS grant 0833).

Notes and references

‡Footnotes relating to the main text should appear here. These might include comments relevant to but not central to the matter under discussion, limited experimental and spectral data, and crystallographic data.

§

§§

etc.

1 N. P. Mankad, *Chem. - A Eur. J.*, 2016, **22**, 5822–5829.
2 L. H. Gade, *Angew. Chemie - Int. Ed.*, 2000, 39, 2658–2678.
3 J. F. Berry and C. C. Lu, *Inorg. Chem.*, 2017, 56, 7577–7581.
4 R. C. Cammarota, L. J. Clouston and C. C. Lu, *Coord. Chem. Rev.*, 2017, **334**, 100–111.
5 N. P. Mankad, *Chem. Commun.*, 2018, **54**, 1291–1302.
6 I. G. Powers and C. Uyeda, *ACS Catal.*, 2017, **7**, 936–958.
7 B. G. Cooper, J. W. Napoline and C. M. Thomas, *Catal. Rev.*, 2012, **54**, 1–40.
8 P. Buchwalter, J. Rosé and P. Braunstein, *Chem. Rev.*, 2015, **115**, 28–126.
9 O. Cooper, C. Camp, J. Pécaut, C. E. Kefalidis, L. Maron, S. Gambarelli and M. Mazzanti, *J. Am. Chem. Soc.*, 2014, **136**, 6716–6723.
10 M. K. Karunananda and N. P. Mankad, *Organometallics*, 2017, **36**, 220–227.
11 M. K. Karunananda and N. P. Mankad, *J. Am. Chem. Soc.*, 2015, **137**, 14598–14601.
12 N. Hidalgo, C. Maya and J. Campos, *Chem. Commun.*, 2019, **55**, 8812–8815.
13 N. Hidalgo, J. J. Moreno, M. Pérez-Jiménez, C. Maya, J. López-Serrano and J. Campos, *Chem. - A Eur. J.*, 2020, chem.202000841.
14 K. M. Gramigna, D. A. Dickie, B. M. Foxman and C. M. Thomas, *ACS Catal.*, 2019, **9**, 3153–3164.
15 I. M. Riddlestone, N. A. Rajabi, J. P. Lowe, M. F. Mahon, S. A. Macgregor and M. K. Whittlesey, *J. Am. Chem. Soc.*, 2016, **138**, 11081–11084.
16 C. M. Thomas, J. W. Napoline, G. T. Rowe and B. M. Foxman, *Chem. Commun.*, 2010, **46**, 5790–5792.
17 M. K. Karunananda, S. R. Parmelee, G. W. Waldhart and N. P. Mankad, *Organometallics*, 2015, **34**, 3857–3864.
18 M. Oishi and H. Suzuki, *Inorg. Chem.*, 2009, **48**, 2349–2351.
19 M. Oishi, M. Oshima and H. Suzuki, *Inorg. Chem.*, 2014, **53**, 6634–6654.
20 M. Oishi, T. Kato, M. Nakagawa and H. Suzuki, *Organometallics*, 2008, **27**, 6046–6049.
21 M. Oishi, M. Kino, M. Saso, M. Oshima and H. Suzuki, *Organometallics*, 2012, **31**, 4658–4661.
22 J. W. Beattie, C. Wang, H. Zhang, J. P. Krogman, B. M. Foxman and C. M. Thomas, *Dalton Trans.*, 2020, **49**, 2407–2411.
23 A. M. Baranger, F. J. Hollander and R. G. Bergman, *J. Am. Chem. Soc.*, 1993, **115**, 7890–7891.
24 A. M. Baranger, F. J. Hollander and R. G. Bergman, *J. Am. Chem. Soc.*, 1993, **115**, 7890–7891.
25 P. L. Dunn, E. P. Beaumier and I. A. Tonks, *Polyhedron*, 2020, **181**, 114471.
26 W. J. Sartain and J. P. Selegue, *J. Am. Chem. Soc.*, 1985,

107, 5818–5820.
27 T. J. Mazzacano and N. P. Mankad, *J. Am. Chem. Soc.*, 2013, **135**, 17258–17261.
28 M. V. Butovskii, C. Döring, V. Bezugly, F. R. Wagner, Y. Grin and R. Kempe, *Nat. Chem.*, 2010, **2**, 741–744.
29 M. Garçon, C. Bakewell, G. A. Sackman, A. J. P. White, R. I. Cooper, A. J. Edwards and M. R. Crimmin, *Nature*, 2019, 574, 390–393.
30 M. V Butovskii, O. L. Tok, F. R. Wagner and R. Kempe, *Angew. Chemie - Int. Ed.*, 2008, **47**, 6469–72.
31 S. Lassalle, R. Jabbour, P. Schiltz, P. Berruyer, T. K. Todorova, L. Veyre, D. Gajan, A. Lesage, C. Thieuleux and C. Camp, *J. Am. Chem. Soc.*, 2019, **141**, 19321–19335.
32 S. Lassalle, R. Jabbour, I. Del Rosal, L. Maron, E. Fonda, L. Veyre, D. Gajan, A. Lesage, C. Thieuleux and C. Camp, *J. Catal.*, 2020, https://doi.org/10.1016/j.jcat.2020.10.016.
33 D. M. Kaphan, R. C. Klet, F. A. Perras, M. Pruski, C. Yang, A. J. Kropf and M. Delferro, *ACS Catal.*, 2018, **8**, 5363–5373.
34 R. Pony Yu, D. Hesk, N. Rivera, I. I. Pelczer and P. J. Chirik, *Nature*, 2016, **529**, 195–199.
35 J. Atzrodt, V. Derdau, W. J. Kerr and M. Reid, *Angew. Chemie - Int. Ed.*, 2018, **57**, 3022–3047.
36 A. D. Becke, *J. Chem. Phys.*, 1993, **98**, 5648–5652.
37 J. P. Perdew, J. A. Chevary, S. H. Vosko, K. A. Jackson, M. R. Pederson, D. J. Singh and C. Fiolhais, *Phys. Rev. B*, 1992, **46**, 6671–6687.
38 D. Andrae, U. Häußermann, M. Dolg, H. Stoll and H. Preuß, *Theor. Chim. Acta*, 1990, **77**, 123–141.
39 A. Bergner, M. Dolg, W. Küchle, H. Stoll and H. Preuß, *Mol. Phys.*, 1993, **80**, 1431–1441.
40 A. W. Ehlers, M. Böhme, S. Dapprich, A. Gobbi, A. Höllwarth, V. Jonas, K. F. Köhler, R. Stegmann, A. Veldkamp and G. Frenking, *Chem. Phys. Lett.*, 1993, **208**, 111–114.
41 R. Ditchfield, W. J. Hehre and J. A. Pople, *J. Chem. Phys.*, 1971, **54**, 720–723.
42 W. J. Hehre, K. Ditchfield and J. A. Pople, *J. Chem. Phys.*, 1972, **56**, 2257–2261.
43 P. C. Hariharan and J. A. Pople, *Theor. Chim. Acta*, 1973, **28**, 213–222.
44 M. M. Francl, W. J. Pietro, W. J. Hehre, J. S. Binkley, M. S. Gordon, D. J. DeFrees and J. A. Pople, *J. Chem. Phys.*, 1982, **77**, 3654–3665.
45 A. E. Reed, L. A. Curtiss and F. Weinhold, *Chem. Rev.*, 1988, **88**, 899–926.
46 S. Grimme, S. Ehrlich and L. Goerigk, *J. Comput. Chem.*, 2011, **32**, 1456–1465.
47 A. V. Marenich, C. J. Cramer and D. G. Truhlar, *J. Phys. Chem. B*, 2009, **113**, 6378–6396.
48 L. Pauling, *J. Am. Chem. Soc.*, 1947, **69**, 542–553.
49 C. Copéret, A. Comas-Vives, M. P. Conley, D. P. Estes, A. Fedorov, V. Mougel, H. Nagae, F. Núñez-Zarur and P. A. Zhizhko, *Chem. Rev.*, 2016, **116**, 323–421.
50 M. Beguerie, C. Dinoi, I. Del Rosal, C. Faradji, G. Alcaraz, L. Vendier and S. Sabo-Etienne, *ACS Catal.*, 2018, **8**, 939–948.
51 L. Castro, E. Kirillov, O. Miserque, A. Welle, L. Haspeslagh, J. F. Carpentier and L. Maron, *ACS Catal.*, 2015, **5**, 416–425.
52 T. Weymuth, E. P. A. Couzijn, P. Chen and M. Reiher, *J. Chem. Theory Comput.*, 2014, **10**, 3092–3103.
53 J. G. Andino, U. J. Kilgore, M. Pink, A. Ozarowski, J. Krzystek, J. Telser, M. H. Baik and D. J. Mindiola, *Chem. Sci.*, 2010, **1**, 351–356.
54 S. Zhang, M. Tamm and K. Nomura, *Organometallics*, 2011, **30**, 2712–2720.
55 J. I. Fostvedt, L. N. Grant, B. M. Kriegel, A. H. Obenhuber, T. D. Lohrey, R. G. Bergman and J. Arnold, *Chem. Sci.*, 2020, **11**, 11613–11632.
56 J. A. Flores, V. N. Cavaliere, D. Buck, B. Pintér, G. Chen, M. G. Crestani, M. H. Baik and D. J. Mindiola, *Chem. Sci.*, 2011, **2**, 1457–1462.
57 B. C. Bailey, H. Fan, E. W. Baum, J. C. Huffman, M. H. Baik and D. J. Mindiola, *J. Am. Chem. Soc.*, 2005, **127**, 16016–16017.
58 B. C. Bailey, H. Fan, J. C. Huffman, M. H. Baik and D. J. Mindiola, *J. Am. Chem. Soc.*, 2007, **129**, 8781–8793.
59 J. S. Vilardo, M. A. Lockwood, L. G. Hanson, J. R. Clark, B. C. Parkin, P. E. Fanwick and I. P. Rothwell, *J. Chem. Soc. - Dalt. Trans.*, 1997, 3353–3362.
60 P. T. Wolczanski, *Organometallics*, 2018, **37**, 505–516.
61 J. J. Carbó, D. García-López, M. Gómez-Pantoja, J. I. González-Pérez, A. Martín, M. Mena and C. Santamaría, *Organometallics*, 2017, **36**, 3076–3083.
62 P. J. Walsh, F. J. Hollander and R. G. Bergman, *J. Am. Chem. Soc.*, 1988, **110**, 8729–8731.
63 C. C. Cummins, S. M. Baxter and P. T. Wolczanski, *J. Am. Chem. Soc.*, 1988, **110**, 8731–8733.
64 M. Findlater, K. M. Schultz, W. H. Bernskoetter, A. Cartwright-Sykes, D. M. Heinekey and M. Brookhart, *Inorg. Chem.*, 2012, **51**, 4672–4678.
65 S. S. Rozenel, R. Padilla, C. Camp and J. Arnold, *Chem. Commun.*, 2014, **50**, 2612–2614.
66 M. Oishi, M. Kino, M. Saso, M. Oshima and H. Suzuki, *Organometallics*, 2012, **31**, 4658–4661.
67 T. M. Gilbert, F. J. Hollander and R. G. Bergman, *J. Am. Chem. Soc.*, 1985, **107**, 3508–3516.
68 Z. E. Clarke, P. T. Maragh, T. P. Dasgupta, D. G. Gusev, A. J. Lough and K. Abdur-Rashid, *Organometallics*, 2006, **25**, 4113–4117.
69 M. J. Hostetler, M. D. Butts and R. G. Bergman, *Organometallics*, 1993, **12**, 65–75.
70 K. Yamamoto, K. Higashida, H. Nagae, H. Tsurugi and K. Mashima, *Helv. Chim. Acta*, 2016, **99**, 848–858.
71 R. Srivastava, E. A. Quadrelli and C. Camp, *Dalton Trans.*, 2020, **49**, 3120–3128.
72 R. Srivastava, R. Moneuse, J. Petit, P.-A. A. Pavard, V. Dardun, M. Rivat, P. Schiltz, M. Solari, E. Jeanneau, L. Veyre, C. Thieuleux, E. A. Quadrelli and C. Camp, *Chem. - A Eur. J.*, 2018, **24**, 4361–4370.